Compatible Triangular Finite Elements Comparison in Thin Plate Analysis

Pedro Miguel de Matos Sanches

November 30, 2011

Abstract

The basis of linear elasticity theory were grounded about two centuries ago. Its generality allowed the establishment of several technical theories, fundamental in several branches of engineering. From this set the theories of beams, plates and shells highlights.

In the present work, moderately thick plate theory is consistently obtained from the three-dimensional continuum equations by imposing static and kinematic restrictions. Thin plate theory – or Kirchhoff's Theory – is then obtained as a particular case of the first.

The Finite Element Method (FEM) has proved to be an important tool in structural analysis and, in particular, in this type of plate. It's constant development aims for solutions, as much as possible, near the exact ones. In this context, convergence analysis is an importante step in the formulation and implementation's assessment of finite elements.

In this dissertation the formulation was revised and four classic compatible triangular finite elements were implemented, *viz.*, the T21, the T18, the HCT12 and the HCT9. Since the first two elements also include nodal curvatures as degrees of freedom, a discussion of boundary kinematic conditions is also presented in order to generate compatible solutions.

The characteristic elemental matrices were symbolically evaluated and systematically expressed by matrix products. To this end, the area coordinates concept was fundamental. In particular, the equivalent nodal force vectors due to distributed effective loads and to linear temperature variations in the thickness of the element were derived.

The numerical examples were chosen so that the results were comparable with the exact solutions given in the bibliography. The implementation was made in MATLAB (2010) environment. From this, important information was extracted allowing relevant conclusions regarding the quality of the several elements in study.

In the conclusions the convergence of several entities, their errors relatively to the exact solutions and the times spent by computational processing with each element were analyzed. Generalized stress diagrams and deformed shapes were also observed and compared with the exact solution.

Keywords: Finite Element Method, thin plates, compatible triangular elements.

1 Thin Plates Theory

Thin plate theory can be consistently obtained from the three-dimensional continuum equations. As usual, the relevant equations should be defined in the domain and on the boundary of the problem.

The *equilibrium equation* is

$$m_{\alpha\beta,\alpha\beta} + \overline{p}_{ef} = 0 \tag{1}$$

where $\overline{p}_{ef}$ represents the *efective load* in the plate's domain given by

$$\overline{p}_{ef} = \overline{p} + \overline{m}_{\alpha,\alpha} \tag{2}$$

being $\overline{p}$ and $\overline{m}_{\alpha}$ the load and the α-component of the moment vector, both applied in the domain, respectively.

The *compatibility equations* in the domain result in the *curvature tensor*, namely

$$\chi_{\alpha\beta} = -w_{,\alpha\beta} \tag{3}$$

It is possible to notice that the shear deformation is not accounted for, as it is on the thick plates theory.

Constitutive relations, including linear temperature variations in the thickness of the plate, can be written as

$$m_{\alpha\beta} = D_f\ ((1-\nu)\,\chi_{\alpha\beta} + \nu\,\chi_{\gamma\gamma}\,\delta_{\alpha\beta}) - \\ - \frac{E\,h^2\,\alpha\,\Delta T_L}{12\,(1-\nu)}\,\delta_{\alpha\beta} \tag{4}$$

On the other hand, the compatibility equations on the *kinematic boundary* are

$$w - \overline{w} = 0 \tag{5a}$$

$$w_{,n} - \overline{w}_{,n} = 0 \tag{5b}$$

$$w_i - \overline{w}_i = 0 \tag{5c}$$

where $\overline{w}$, $\overline{w}_{,n}$ and $\overline{w}_i$ are the *prescribed displacement*, *prescribed normal derivative of the transversal displacement*

and *prescribed displacement at the ith corner point*, respectively.

On the *static boundary*, the equilibrium conditions are

$$r_n - \overline{r}_n^{\Gamma} = 0 \tag{6a}$$

$$m_{nn} - \overline{m}_{nn}^{\Gamma} = 0 \tag{6b}$$

$$P_i - \overline{P}_i^{\Gamma} = 0 \tag{6c}$$

where $\overline{r}_n^{\Gamma}$, $\overline{m}_{nn}^{\Gamma}$ and $\overline{P}_i^{\Gamma}$ are the *normal efective load*, *normal moment* and the *discontinuity of normal tangential moment* applied at the corner point i, prescribed on the static boundary, respectively. Also, the normal efective load prescribed on the static boundary, $\overline{r}_n^{\Gamma}$, is given by

$$\overline{r}_n^{\Gamma} = \overline{p}^{\Gamma} + \overline{m}_{nt,t}^{\Gamma} - \overline{m}_{nn} \tag{7}$$

being $\overline{p}^{\Gamma}$ the *applied load on the boundary* and $\overline{m}_{nn} = \overline{m}_{\alpha}\, n_{\alpha}$ is the *effect on the boundary of the applied moment in the domain.*

2 Finite Element Method

In the traditional form of the FEM, the displacement approximation for the generic element (e) is given by

$$w^{(\mathrm{e})} = \boldsymbol{\Psi}^{(\mathrm{e})}\, \mathbf{d}^{(\mathrm{e})} \tag{8}$$

where $\boldsymbol{\Psi}^{(\mathrm{e})}$ is the *element approximation functions matrix* and $\mathbf{d}^{(\mathrm{e})}$ is the *element generalized displacements vector.* The compatibility equation relates the *element curvatures vector*, $\boldsymbol{\chi}^{(\mathrm{e})}$, with the element nodal displacements vector

$$\boldsymbol{\chi}^{(\mathrm{e})} = \mathbf{B}^{(\mathrm{e})}\, \mathbf{d}^{(\mathrm{e})} \tag{9}$$

where $\mathbf{B}^{(\mathrm{e})}$ is the matrix gathering the element approximations functions derivatives

$$\mathbf{B}^{(\mathrm{e})} = \boldsymbol{\partial}\, \boldsymbol{\Psi}^{(\mathrm{e})} \tag{10}$$

The constitutive relation allows obtaining the *element moment vector*, $\mathbf{m}^{(\mathrm{e})}$, by taking into account the curvatures due to *linear temperature variations vector*, $\boldsymbol{\chi}_{\Delta T}^{(\mathrm{e})}$, as

$$\mathbf{m}^{(\mathrm{e})} = \mathbf{D}^{(\mathrm{e})} \left(\boldsymbol{\chi}^{(\mathrm{e})} - \boldsymbol{\chi}_{\Delta T}^{(\mathrm{e})} \right) \tag{11}$$

where $\mathbf{D}^{(\mathrm{e})}$ is the *element stiffness constitutive matrix.*

The element FEM equation is given by

$$\mathbf{K}^{(\mathrm{e})}\, \mathbf{d}^{(\mathrm{e})} = \mathbf{f}^{(\mathrm{e})} \tag{12}$$

where the *element stiffness matrix*, $\mathbf{K}^{(\mathrm{e})}$, and the *element nodal equivalent force vector*, $\mathbf{f}^{(\mathrm{e})}$, are, respectively,

$$\mathbf{K}^{(\mathrm{e})} = \int_{\Omega^{(\mathrm{e})}} \mathbf{B}^{(\mathrm{e})T}\, \mathbf{D}^{(\mathrm{e})}\, \mathbf{B}^{(\mathrm{e})}\, \mathrm{d}\Omega^{(\mathrm{e})} \tag{13a}$$

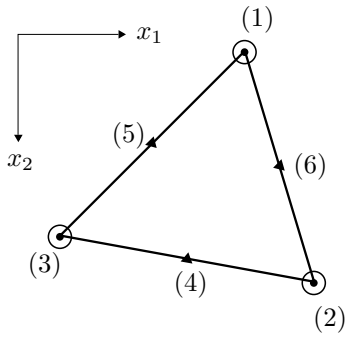

$\odot$ $(w - w_{,1} - w_{,2} - w_{,11} - w_{,12} - w_{,22})$

▲ $w_{,n}$

Figure 1: T21 element.

$$\mathbf{f}^{(\mathrm{e})} = \int_{\Omega^{(\mathrm{e})}} \boldsymbol{\Psi}^{(\mathrm{e})T}\, \overline{p}_{ef}\, \mathrm{d}\Omega^{(\mathrm{e})} + \int_{\Gamma_t^{(\mathrm{e})}} \left(\boldsymbol{\Psi}^{(\mathrm{e})T}\, \overline{r}_n^{\Gamma} - \frac{\partial\, \boldsymbol{\Psi}^{(\mathrm{e})T}}{\partial\, n}\, \overline{m}_{nn}^{\Gamma} \right) \mathrm{d}\Gamma_t^{(\mathrm{e})} + \int_{\Omega^{(\mathrm{e})}} \mathbf{B}^{(\mathrm{e})T}\, \mathbf{D}^{(\mathrm{e})}\, \boldsymbol{\chi}_{\Delta T}^{(\mathrm{e})}\, \mathrm{d}\Omega^{(\mathrm{e})} \tag{13b}$$

The first term of the second member of (13b) represents the contribution due to the efective load distributed in the domain. The second and third terms represents the contributions due to the generalized loads applied on the static boundary and due to the linear temperature variations, respectively.

After assembling all elemental matrices, *vide* Zienkiewicz *et al.* (2005, page 5), the global system equation – which defines the equivalent nodal forces equilibrium conditions – is obtained

$$\mathbf{K}\, \mathbf{d} = \mathbf{f} \tag{14}$$

This equation is enforcing the equilibrium in the domain and on the static boundary.

3 T21 Element Formulation

3.1 Approximation Functions

The T21 is a six node finite element with twenty one degrees of freedom (dof), where each vertex node has six dof and each of the mid-side nodes have one dof, as presented in figure 1. This element was proposed by several authors, *e.g.*, Argyris *et al.* (1968) and Bell (1969).

As shown, the vertex degrees of freedom include transversal displacement, its first order partial derivatives and flexure and torsion curvatures. On the other hand, mid-side nodes only include the normal derivative.

The approximation for the element displacement field is given by

$$w^{(\mathrm{e})} = \mathbf{P}\, \boldsymbol{\alpha}^{(\mathrm{e})} \tag{15}$$

where $\mathbf{P}$ is the *matrix that gathers the approximation modes* and includes the twenty one terms of the complete quintic

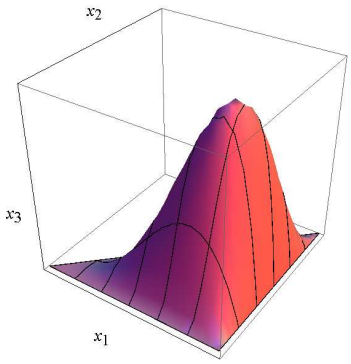

Figure 2: $\psi_{20}^{(e)}(L_1, L_2, L_3)$ approximation function.

polynomial and $\boldsymbol{\alpha}^{(e)}$ is an element vector that includes the twenty one *approximation weights*.

Using area coordinates, the $\mathbf{P}$ matrix is given by

$$\begin{aligned}\mathbf{P} = \big[&L_1^5 \quad L_2^5 \quad L_3^5 \\ &L_1^4 L_2 \quad L_1^4 L_3 \quad L_2^4 L_1 \quad L_2^4 L_3 \quad L_3^4 L_1 \quad L_3^4 L_2 \\ &L_1^3 L_2^2 \quad L_1^3 L_3^2 \quad L_2^3 L_1^2 \quad L_2^3 L_3^2 \quad L_3^3 L_1^2 \quad L_3^3 L_2^2 \\ &L_1^3 L_2 L_3 \quad L_2^3 L_1 L_3 \quad L_3^3 L_1 L_2 \quad L_1 L_2^2 L_3^2 \\ &L_2 L_1^2 L_3^2 \quad L_3 L_1^2 L_2^2\big] \end{aligned} \tag{16}$$

and the $\boldsymbol{\alpha}^{(e)}$ vector is

$$\boldsymbol{\alpha}^{(e)T} = \{\alpha_1 \quad \alpha_2 \quad \alpha_3 \quad \dots \quad \alpha_{21}\} \tag{17}$$

The relation between the approximation weights, $\boldsymbol{\alpha}^{(e)}$, and the element generalized nodal displacements, $\mathbf{d}^{(e)}$, can be written in matrix form as

$$\mathbf{d}^{(e)} = \mathbf{A}^{(e)}\,\boldsymbol{\alpha}^{(e)} \Leftrightarrow \boldsymbol{\alpha}^{(e)} = \mathbf{A}^{(e)-1}\mathbf{d}^{(e)} \tag{18}$$

where $\mathbf{A}^{(e)}$ is a linear operator that maps $\boldsymbol{\alpha}^{(e)}$ onto $\mathbf{d}^{(e)}$.

Substituting (18) in (15) leads to

$$w^{(e)} = \mathbf{P}\mathbf{A}^{(e)-1}\mathbf{d}^{(e)} \Leftrightarrow w^{(e)} = \boldsymbol{\Psi}^{(e)}\mathbf{d}^{(e)} \tag{19}$$

The matrix $\mathbf{A}^{(e)}$ only involves element geometrical properties – expressed by b_i and c_i – and, therefore, can be determined explicitly. To obtain the approximation functions matrix, $\boldsymbol{\Psi}^{(e)}$, the use of Mathematica software (Wolfram Research, 2010) was fundamental. The majority of the expressions obtained are to extensive to be shown, hence it will only be reproduced here one example of a simpler expression associated at the normal derivative for the i side, namely

$$\psi_{18+i}^{(e)} = -\frac{32\,A^{(e)}}{l_i} L_i\,L_j^2\,L_k^2. \tag{20}$$

Here $A^{(e)}$ is the element area and l_i is the length of the ith side. Both of these can be expressed as a function of b_i and c_i. One example of a mid-side approximation function is shown in figure 2.

3.2 Element Stiffness Matrix

The $\mathbf{B}^{(e)}$ matrix presented in (10), used to obtain the curvature element vector, can be expressed by a third degree complete polinomial base in the two-dimensional space, thus having dimension ten, *e.g.*,

$$\begin{aligned}\mathbf{L} = \big[&L_1^3 \quad L_2^3 \quad L_3^3 \quad L_1^2 L_2 \quad L_1^2 L_3 \quad L_1 L_2^2 \\ &L_2^2 L_3 \quad L_1 L_3^2 \quad L_2 L_3^2 \quad L_1 L_2 L_3\big]\end{aligned} \tag{21}$$

Therefore, $\mathbf{B}^{(e)}$ can be expressed by

$$\mathbf{B}^{(e)} = \frac{1}{4A^{(e)2}}\,\mathbf{F}\,\mathbf{Q}^{(e)} = \frac{1}{4A^{(e)2}} \begin{bmatrix}\mathbf{L} & 0 & 0\\ 0 & \mathbf{L} & 0\\ 0 & 0 & \mathbf{L}\end{bmatrix} \begin{bmatrix}\mathbf{Q}_{11}^{(e)}\\ \mathbf{Q}_{22}^{(e)}\\ \mathbf{Q}_{12}^{(e)}\end{bmatrix} \tag{22}$$

where $\mathbf{Q}_{11}^{(e)}$, $\mathbf{Q}_{22}^{(e)}$ and $\mathbf{Q}_{12}^{(e)}$ are (10×21) matrices that stores the curvatures approximation functions coefficients.

Using (13a), the element stiffness matrix can by written as

$$\mathbf{K}^{(e)} = \frac{1}{8A^{(e)3}}\mathbf{Q}^{(e)T}\mathbf{S}^{(e)}\mathbf{Q}^{(e)} \tag{23}$$

where

$$\mathbf{S}^{(e)} = \frac{1}{2A^{(e)}}\int_{\Omega^{(e)}} \mathbf{F}^T\mathbf{D}^{(e)}\mathbf{F}\,\mathrm{d}\Omega^{(e)} \tag{24}$$

with

$$\mathbf{F}^T\mathbf{D}^{(e)}\mathbf{F} = \begin{bmatrix} D_{11}^{(e)}\mathbf{L}^T\mathbf{L} & D_{12}^{(e)}\mathbf{L}^T\mathbf{L} & 0\\ D_{21}^{(e)}\mathbf{L}^T\mathbf{L} & D_{22}^{(e)}\mathbf{L}^T\mathbf{L} & 0\\ 0 & 0 & D_{33}^{(e)}\mathbf{L}^T\mathbf{L}\end{bmatrix} \tag{25}$$

Defining the $\mathbf{R}$ matrix, that can be explicitly evaluated, as

$$\mathbf{R} = \frac{1}{2A^{(e)}}\int_{\Omega^{(e)}} \mathbf{L}^T\mathbf{L}\,\mathrm{d}\Omega^{(e)} \tag{26}$$

we have

$$\mathbf{S}^{(e)} = \begin{bmatrix} D_{11}^{(e)}\mathbf{R} & D_{12}^{(e)}\mathbf{R} & 0\\ D_{21}^{(e)}\mathbf{R} & D_{22}^{(e)}\mathbf{R} & 0\\ 0 & 0 & D_{33}^{(e)}\mathbf{R}\end{bmatrix} \tag{27}$$

Finally, the element stiffness matrix is

$$\begin{aligned}\mathbf{K}^{(e)} &= \frac{1}{8A^{(e)3}}\mathbf{Q}^{(e)T}\mathbf{S}^{(e)}\mathbf{Q}^{(e)} = \\ &= \frac{1}{8A^{(e)3}}\Big(D_{11}^{(e)}\mathbf{Q}_{11}^{(e)T}\mathbf{R}\,\mathbf{Q}_{11}^{(e)} + \\ &+ D_{12}^{(e)}\mathbf{Q}_{11}^{(e)T}\mathbf{R}\,\mathbf{Q}_{22}^{(e)} + D_{21}^{(e)}\mathbf{Q}_{22}^{(e)T}\mathbf{R}\,\mathbf{Q}_{11}^{(e)} + \\ &+ D_{22}^{(e)}\mathbf{Q}_{22}^{(e)T}\mathbf{R}\,\mathbf{Q}_{22}^{(e)} + D_{33}^{(e)}\mathbf{Q}_{12}^{(e)T}\mathbf{R}\,\mathbf{Q}_{12}^{(e)}\Big)\end{aligned} \tag{28}$$

3.3 Element Force Vector

Since this is a six node element, the equivalent nodal force vector, $\mathbf{f}^{(e)}$, can be implemented allowing quadratic distributed effective loads, $\overline{p}_{ef}$, and differential temperature variations, ΔT. Notice that six points allow the definition of a quadratic polynomial in the two-dimensional space.

This vector, like the stiffness matrix, can be explicitly evaluated in area coordinates and will be the sum of the effective load and the temperature variation contributions, *i.e.*,

$$\mathbf{f}^{(\mathrm{e})} = \mathbf{f}^{(\mathrm{e})}_{\overline{p}_{ef}} + \mathbf{f}^{(\mathrm{e})}_{\Delta T} \tag{29}$$

For the effective load, the $\mathbf{f}^{(\mathrm{e})}_{\overline{p}_{ef}}$ vector is given by the first term of the second member of (13b). The quadratic load, $\overline{p}^{(\mathrm{e})}_{ef}$, is written in area coordinates by

$$\overline{p}^{(\mathrm{e})}_{ef}\left(L_1, L_2, L_3\right) = \mathbf{\Psi}^Q\, \overline{\mathbf{p}}^{(\mathrm{e})}_{ef} \tag{30}$$

where $\mathbf{\Psi}^Q$ is a vector that groups the quadratic shape functions given by

$$\psi^Q_i = \left(L_i - L_j - L_k\right) L_i \tag{31a}$$

$$\psi^Q_{i+3} = 4 L_j L_k \tag{31b}$$

and $\overline{\mathbf{p}}^{(\mathrm{e})}_{ef}$ groups the load values at the element nodes.

Also, the $\mathbf{\Psi}^Q$ vector is written by

$$\mathbf{\Psi}^Q = \mathbf{P}^Q \mathbf{Y}^Q \tag{32}$$

where $\mathbf{P}^Q$ is a quadratic polynomial base

$$\mathbf{P}^Q = \begin{bmatrix} L_1^2 & L_2^2 & L_3^2 & L_1 L_2 & L_1 L_3 & L_2 L_3 \end{bmatrix} \tag{33}$$

Therefore, the $\mathbf{f}^{(\mathrm{e})}_{\overline{p}_{ef}}$ vector is given by

$$\mathbf{f}^{(\mathrm{e})}_{\overline{p}_{ef}} = \int_{\Omega^{(e)}} \mathbf{\Psi}^{(\mathrm{e})T} \mathbf{\Psi}^Q \,\mathrm{d}\Omega^{(e)}\, \overline{\mathbf{p}}^{(e)}_{ef} = \\ = \mathbf{A}^{(e)-T} \int_{\Omega^{(e)}} \mathbf{P}^T \mathbf{P}^Q \,\mathrm{d}\Omega^{(e)}\, \mathbf{Y}^Q \overline{\mathbf{p}}^{(e)}_{ef} \tag{34}$$

Defining the $\mathbf{Z}$ matrix, that can be explicitly evaluated, by

$$\mathbf{Z} = \frac{1}{A^{(\mathrm{e})}} \int_{\Omega^{(e)}} \mathbf{P}^T \mathbf{P}^Q \,\mathrm{d}\Omega^{(e)} \tag{35}$$

it is possible to write

$$\mathbf{f}^{(\mathrm{e})}_{\overline{p}_{ef}} = A^{(\mathrm{e})} \mathbf{A}^{(e)-T} \mathbf{Z}\, \mathbf{Y}^Q \overline{\mathbf{p}}^{(e)}_{ef} \tag{36}$$

In the same way, the $\mathbf{f}^{(\mathrm{e})}_{\Delta T}$ vector generalization is given by the last term of the second member of (13b). The quadratic temperature variation, $\Delta T^{(\mathrm{e})}$, is written in area coordinates by

$$\Delta T^{(\mathrm{e})}\left(L_1, L_2, L_3\right) = \mathbf{\Psi}^Q \Delta \mathbf{T}^{(\mathrm{e})} \tag{37}$$

where $\Delta \mathbf{T}^{(\mathrm{e})}$ is a vector that groups the temperature values at the element nodes.

Since this solicitation only generates initial flexure curvatures, we define the $\mathbf{v}$ vector as

$$\mathbf{v}^T = \begin{Bmatrix} 1 & 1 & 0 \end{Bmatrix}$$

Then the curvatures vector caused by the quadratic temperature variation can be written as

$$\boldsymbol{\chi}^{(\mathrm{e})}_{\Delta T} = \mathbf{v} \frac{\alpha}{h} \Delta T^{(\mathrm{e})} = \frac{\alpha}{h}\, \mathbf{v}\, \mathbf{P}^Q \mathbf{Y}^Q \Delta \mathbf{T}^{(\mathrm{e})} \tag{38}$$

The $\mathbf{f}^{(\mathrm{e})}_{\Delta T}$ vector is now given by

$$\mathbf{f}^{(\mathrm{e})}_{\Delta T} = \frac{1}{4 A^{(\mathrm{e})2}} \frac{\alpha}{h} \mathbf{Q}^{(\mathrm{e})T} \\ \int_{\Omega^{(\mathrm{e})}} \mathbf{F}^T \mathbf{D}^{(\mathrm{e})}_{\mathbf{v}}\, \mathbf{P}^Q \,\mathrm{d}\Omega^{(\mathrm{e})} \mathbf{Y}^Q \Delta \mathbf{T}^{(\mathrm{e})} \tag{39}$$

Matrix $\mathbf{H}^{(\mathrm{e})}$ is introduced as

$$\mathbf{H}^{(\mathrm{e})} = \int_{\Omega^{(\mathrm{e})}} \mathbf{F}^T \mathbf{D}^{(\mathrm{e})}_{\mathbf{v}}\, \mathbf{P}^Q \,\mathrm{d}\Omega^{(\mathrm{e})} = \\ = \int_{\Omega^{(\mathrm{e})}} \begin{bmatrix} \mathbf{L}^T \mathbf{P}^Q \left(D^{(\mathrm{e})}_{11} + D^{(\mathrm{e})}_{12}\right) \\ \mathbf{L}^T \mathbf{P}^Q \left(D^{(\mathrm{e})}_{21} + D^{(\mathrm{e})}_{22}\right) \\ 0 \end{bmatrix} \mathrm{d}\Omega^{(\mathrm{e})} = \\ = A^{(\mathrm{e})} \begin{bmatrix} \mathbf{M} \left(D^{(\mathrm{e})}_{11} + D^{(\mathrm{e})}_{12}\right) \\ \mathbf{M} \left(D^{(\mathrm{e})}_{21} + D^{(\mathrm{e})}_{22}\right) \\ 0 \end{bmatrix} \tag{40}$$

where matrix $\mathbf{M}$ can be explicitly evaluated by

$$\mathbf{M} = \frac{1}{A^{(\mathrm{e})}} \int_{\Omega^{(\mathrm{e})}} \mathbf{L}^T \mathbf{P}^Q \,\mathrm{d}\Omega^{(\mathrm{e})} \tag{41}$$

Finally, the equivalent nodal force vector due to quadratic differential temperature variations in the element domain is given by

$$\mathbf{f}^{(\mathrm{e})}_{\Delta T} = \frac{1}{4 A^{(\mathrm{e})}} \frac{\alpha}{h} \left(\mathbf{Q}^{(\mathrm{e})T}_{11} \mathbf{M} \left(D^{(\mathrm{e})}_{11} + D^{(\mathrm{e})}_{12}\right) + \\ + \mathbf{Q}^{(\mathrm{e})T}_{22} \mathbf{M} \left(D^{(\mathrm{e})}_{21} + D^{(\mathrm{e})}_{22}\right) \right) \mathbf{Y}^Q \Delta \mathbf{T}^{(\mathrm{e})} \tag{42}$$

3.4 Element Compatibility

To generate a compatible solutions space, the compatibility in the domain and on the boundary has to be satisfied, generating a C^1 class approximation.

In the domain, the approximation is generated by a polynomial, so the approximation itself and all its derivatives are continuous. Therefore, the element is C^∞ in the domain.

Compatibility on the boundary between elements has to be proven by assuring the continuity of the displacement approximation function and its normal and tangential derivatives.

Since w is a fifth degree function, we need six parameters to define the approximation along a straight line. In each vertex node we prescribe the displacement, w, the first order derivative, $w_{,t}$, and the curvature, χ_{tt}, making the six necessary parameters, see figure 3.

The approximation's normal derivative is a fourth degree polynomial so five parameters are needed to ensure its compatibility. In each vertex node we prescribe the normal derivative, $w_{,n}$, and the curvature, χ_{nt}, making four parameters. The fifth one will be the normal derivative in the mid-side node, see figure 4.

On the boundary between elements, the tangential derivative is also compatible since the displacement of contiguous elements is exactly the same.

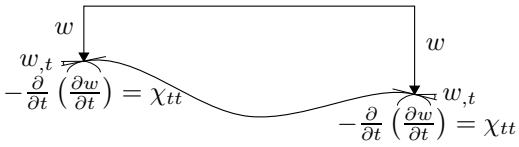

Figure 3: Displacement compatibility of T21 element.

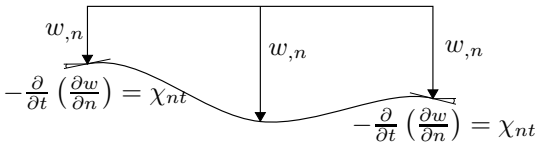

Figure 4: Normal derivative compatibility of T21 element.

Lastly, to satisfy the compatibility conditions on the kinematic boundary we have to impose, not only the usual degrees of freedom, like displacements and their first order partial derivatives, but also curvatures.

In general, the conditions should be imposed for prescribed quantities like, for example, $w = \overline{w}$. In this case, in order to simplify the exposition only use homogeneous conditions will be used.

For three common border types the homogeneous boundary conditions are:

- Simply supported edge: $w = 0$, $(-w_{,t}) = 0$ and $(-w_{,tt}) = 0$.
- Clamped edge: $w = 0$, $(-w_{,n}) = 0$, $(-w_{,t}) = 0$, $(-w_{,nt}) = 0$ and $(-w_{,tt}) = 0$.
- Sliding clamped edge: $(-w_{,n}) = 0$ and $(-w_{,nt}) = 0$.

Since the number of conditions being used is exactly the same as in the case of the boundary between elements, the compatibility on the kinematic boundary is also demonstrated.

4 T18 Element Formulation

4.1 Approximation Functions

The T18 finite element derives from the preceding one by suppressing the mid-side nodes. Therefore, the resulting element has eighteen degrees of freedom by matching those of the T21 element vertex nodes. This element also appears in the same papers where T21 was proposed.

To maintain the displacements' and first order derivatives' compatibility we impose a cubic variation in the normal derivative along the element sides, defined by the nodal parameters.

The restriction relation between the nodal displacements of mid-side nodes, $\mathbf{d}_s^{(\mathrm{e})}$, and the nodal displacements of vertex nodes, $\mathbf{d}_f^{(\mathrm{e})}$, can be written by

$$\mathbf{d}_s^{(\mathrm{e})} = \mathbf{G}\,\mathbf{d}_f^{(\mathrm{e})} \tag{43}$$

with

$$\mathbf{d}_s^{(\mathrm{e})} = \begin{Bmatrix} (w,_n)_1 \\ (w,_n)_2 \\ (w,_n)_3 \end{Bmatrix} \quad \text{and} \quad \mathbf{d}_f^{(\mathrm{e})} = \begin{Bmatrix} \mathbf{d}_1^{(\mathrm{e})} \\ \mathbf{d}_2^{(\mathrm{e})} \\ \mathbf{d}_3^{(\mathrm{e})} \end{Bmatrix} \tag{44}$$

where

$$\mathbf{d}_i^{(\mathrm{e})} = \begin{Bmatrix} w_i \\ -w_{,1i} \\ -w_{,2i} \\ -w_{,11i} \\ -w_{,12i} \\ -w_{,22i} \end{Bmatrix} \tag{45}$$

and $\mathbf{G}$ is the restriction's matrix given by

$$\mathbf{G} = \begin{bmatrix} 0 & \mathbf{G}_{12} & \mathbf{G}_{13} \\ \mathbf{G}_{21} & 0 & \mathbf{G}_{23} \\ \mathbf{G}_{31} & \mathbf{G}_{32} & 0 \end{bmatrix} \tag{46}$$

where the $\mathbf{G}_{ij}$ submatrices are

$$\mathbf{G}_{12} = [0 \;\; C_{11} \;\; C_{21} \;\; -C_{31} \;\; C_{41} \;\; C_{31}] \tag{47a}$$
$$\mathbf{G}_{13} = [0 \;\; C_{11} \;\; C_{21} \;\; C_{31} \;\; -C_{41} \;\; -C_{31}] \tag{47b}$$
$$\mathbf{G}_{21} = [0 \;\; C_{12} \;\; C_{22} \;\; C_{32} \;\; -C_{42} \;\; -C_{32}] \tag{47c}$$
$$\mathbf{G}_{23} = [0 \;\; C_{12} \;\; C_{22} \;\; -C_{32} \;\; C_{42} \;\; C_{32}] \tag{47d}$$
$$\mathbf{G}_{31} = [0 \;\; C_{13} \;\; C_{23} \;\; -C_{33} \;\; C_{43} \;\; C_{33}] \tag{47e}$$
$$\mathbf{G}_{32} = [0 \;\; C_{13} \;\; C_{23} \;\; C_{33} \;\; -C_{43} \;\; -C_{33}] \tag{47f}$$

The C_{ij} constants are defined, for the k side, as follows

$$C_{1k} = \frac{1}{2} n_{1k} \tag{48a}$$
$$C_{2k} = \frac{1}{2} n_{2k} \tag{48b}$$
$$C_{3k} = \frac{h_k}{8} n_{1k} n_{2k} \tag{48c}$$
$$C_{4k} = \frac{h_k}{8} \left(n_{1k}^2 - n_{2k}^2\right) \tag{48d}$$

where n_1 and n_2 are the k's side normal vector components along x_1 and x_2 axis, respectively.

Dividing the T21 approximation function matrix, $\mathbf{\Psi}^{(\mathrm{e})}$, into two submatrices grouping the approximation functions corresponding to the vertex nodes, $\mathbf{\Psi}_f^{(\mathrm{e})}$, and to the mid-side nodes, $\mathbf{\Psi}_s^{(\mathrm{e})}$, and proceeding in the same way for the equivalent nodal force vector, $\mathbf{d}^{(\mathrm{e})}$, we have

$$w^{(\mathrm{e})} = \mathbf{\Psi}^{(\mathrm{e})}\mathbf{d}^{(\mathrm{e})} = \begin{bmatrix} \mathbf{\Psi}_f^{(\mathrm{e})} & \mathbf{\Psi}_s^{(\mathrm{e})} \end{bmatrix} \begin{Bmatrix} \mathbf{d}_f^{(\mathrm{e})} \\ \mathbf{d}_s^{(\mathrm{e})} \end{Bmatrix} = \\ = \left[\mathbf{\Psi}_f^{(\mathrm{e})} + \mathbf{\Psi}_s^{(\mathrm{e})}\mathbf{G}\right] \mathbf{d}_f^{(\mathrm{e})} = \mathbf{\Psi}_{\mathrm{T18}}^{(\mathrm{e})} \mathbf{d}_f^{(\mathrm{e})} \tag{49}$$

Thus, it is possible to extract the T18's approximation functions, $\mathbf{\Psi}_{\mathrm{T18}}^{(\mathrm{e})}$, by

$$\mathbf{\Psi}_{\mathrm{T18}}^{(\mathrm{e})} = \mathbf{\Psi}_f^{(\mathrm{e})} + \mathbf{\Psi}_s^{(\mathrm{e})}\mathbf{G} \tag{50}$$

and the relation between the vector that groups the nodal displacements and their derivatives for the T21 element, $\mathbf{d}^{(\mathrm{e})}$, with the homonymous of the T18 element, $\mathbf{d}^{(\mathrm{e})}_{\mathrm{T18}}$,

$$\mathbf{d}^{(\mathrm{e})} = \begin{Bmatrix} \mathbf{d}_f^{(\mathrm{e})} \\ \mathbf{d}_s^{(\mathrm{e})} \end{Bmatrix} = \begin{bmatrix} \mathbf{I}_{18} \\ \mathbf{G} \end{bmatrix} \mathbf{d}_f^{(\mathrm{e})} = \mathbf{G_I} \mathbf{d}^{(\mathrm{e})}_{\mathrm{T18}} \tag{51}$$

where $\mathbf{I}_{18}$ represents the identity matrix with dimension (18×18).

4.2 Element Stiffness Matrix

The procedure to evaluate this matrix is very similar to what has been done to the T21 element. The expression given by (28) is still valid and the difference is only in the in the $\mathbf{Q}^{(\mathrm{e})}$ matrix that now has the dimension (30×18). Both $\mathbf{F}$ and $\mathbf{L}$ matrices are element independent, therefore the $\mathbf{R}$ is also element independent.

4.3 Element Force Vector

Once again, the T18's element force vector formulation stays close to what has been made for the T21 element. However, in this case, since there only are two nodes in each element side, making a total of three nodes, only linear loads in the two-dimensional space can be defined. Therefore, the equation given by (29) is still valid but each contribution is now, at most, linear.

The effective load, $\overline{p}^{(\mathrm{e})}_{ef}$, defined in (30) is now expressed by linear shape functions, ψ_i^L, that can be grouped in a single vector, $\mathbf{\Psi}^L$, given by

$$\mathbf{\Psi}^L = \mathbf{P}^L \mathbf{Y}^L = \mathbf{P}^L \mathbf{I}_3 = \mathbf{P}^L \tag{52}$$

where $\mathbf{P}^L$ represents a linear polynomial base, independent of the element, given by

$$\mathbf{P}^L = \begin{bmatrix} L_1 & L_2 & L_3 \end{bmatrix} \tag{53}$$

and the $\mathbf{Y}^L$ matrix is the identity matrix of dimension (3×3), $\mathbf{I}_3$.

Consider that the T18 approximation matrixes, given by (50), are now written as a function of the T21 base (16) in the form

$$\mathbf{\Psi}^{(\mathrm{e})}_{\mathrm{T18}} = \mathbf{P}\,\mathbf{W} \tag{54}$$

where the $\mathbf{W}$ matrix has dimension (21×18).

Following a similar procedure to that made in (34) we have

$$\mathbf{f}^{(\mathrm{e})}_{\overline{p}_{ef}} = \int_{\Omega^{(e)}} \mathbf{\Psi}^{(\mathrm{e})}_{\mathrm{T18}} \mathbf{\Psi}^L \,\mathrm{d}\Omega^{(e)}\, \overline{\mathbf{p}}^{(e)}_{ef} = \\ = \mathbf{W}^{(e)T} \int_{\Omega^{(e)}} \mathbf{P}^T \mathbf{P}^L \,\mathrm{d}\Omega^{(e)}\, \mathbf{I}_3\, \overline{\mathbf{p}}^{(e)}_{ef} \tag{55}$$

The procedure to obtain the element nodal force vector due to temperature variations is obtained by (42), again with the suppression of the $\mathbf{Y}^L$ matrix.

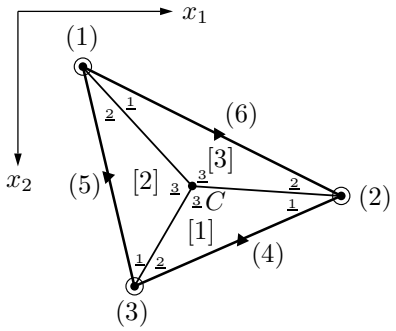

Figure 5: HCT12 element division in subelements.

4.4 Element Compatibility

The necessary conditions regarding the domain and the kinematic boundary are the same as those presented for the T21 element.

The same procedure applies when ensuring the transversal displacement and tangencial derivative compatibility but when it comes to the normal derivative, a change has to be pointed out. In this case, the normal derivative approximation is cubic and it is required to prescribe four parameters. These are the normal derivative, $w_{,n}$, and the torsion curvatures, $w_{,ns}$, of the element nodes along each edge.

5 HCT12 Element Formulation

5.1 Approximation Functions

The HCT12 element has the same six nodes of the T21 element but only a total of twelve degrees of freedom. In this case, the vertex nodes do not have curvatures as dof's. Instead, they only have three dof's, namely, w, $(-w_{,1})$ and $(-w_{,2})$. Each mid-side node has one dof – the normal derivative, $w_{,n}$. This element was mentioned in Clough and Tocher (1966), but only described and numerically assessed in Clough and Felippa (1969).

Inside each element, the approximation for the displacement field is made by "piecewise functions". Each triangular element is divided in three subelements – *vide* figure 5 – and in each one of them a complete cubic polynomial is assumed for the displacement, $w\,(x_1, x_2)$. Its base has, in the two-dimensional space, ten terms. These are taken, in cartesian coordinates, from Pascal's triangle

$$\begin{array}{ccccc} & & 1 & & \\ & & x_1 & x_2 & \\ & x_1^2 & x_1 x_2 & x_2^2 & \\ x_1^3 & x_1^2 x_2 & x_1 x_2^2 & x_2^3 & \end{array}$$

In figure 5, point C represents the center of the element, $[i]$ is the subelement number, $\underline{i}$ are the subelement nodes and (i) are the element nodes.

To completely define the displacement's approximation in the element, $3 \times 10 = 30$ parameters are needed. Since it

only has twelve degrees of freedom, $30-12=18$ restrictions have to be imposed to the three subelements' approximations, in a way that C^1 continuity of the approximation inside the element is guaranteed.

Therefore, at the center C, we shall impose six restrictions[1], namely,

$$w^{[1]} = w^{[2]} \tag{56a}$$
$$w^{[2]} = w^{[3]} \tag{56b}$$
$$-w^{[1]}_{,1} = -w^{[2]}_{,1} \tag{56c}$$
$$-w^{[2]}_{,1} = -w^{[3]}_{,1} \tag{56d}$$
$$-w^{[1]}_{,2} = -w^{[2]}_{,2} \tag{56e}$$
$$-w^{[2]}_{,2} = -w^{[3]}_{,2} \tag{56f}$$

Similarly, in the element's (i) vertex node, we shall impose three restriction in a total of nine, namely,

$$w^{[j]} = w^{[k]} \tag{57a}$$
$$-w^{[j]}_{,1} = -w^{[k]}_{,1} \tag{57b}$$
$$-w^{[j]}_{,2} = -w^{[k]}_{,2} \tag{57c}$$

where the i, j and k indexes cyclically permute.

Finally, at the middle of the side that joins the center C to the (i) vertex node of the element, we shall impose one more restriction in a total of three, *i.e.*,

$$w^{[j]}_{,n} = -w^{[k]}_{,n} \tag{58}$$

with the i, j and k indexes also cyclically permuting.

With the division of the element in subelements, we have the degrees of freedom in the element nodes and in the center C. This last ones will be eliminated in due time.

Therefore the vector that groups the nodal degrees of freedom, $\mathbf{d}^{(\mathrm{e})}$, is defined as

$$\mathbf{d}^{(\mathrm{e})T} = \left\{ \mathbf{d}^{(\mathrm{e})}_{(1)} \; \mathbf{d}^{(\mathrm{e})}_{(2)} \; \mathbf{d}^{(\mathrm{e})}_{(3)} \; d^{(\mathrm{e})}_{(4)} \; d^{(\mathrm{e})}_{(5)} \; d^{(\mathrm{e})}_{(6)} \right\} \tag{59}$$

where, for $i=\{1,2,3\}$, we have

$$\mathbf{d}^{(\mathrm{e})}_{(i)} = \begin{Bmatrix} w \\ -w_{,1} \\ -w_{,2} \end{Bmatrix}_{(i)} = \begin{Bmatrix} d^{(\mathrm{e})}_{3(i-1)+1} \\ d^{(\mathrm{e})}_{3(i-1)+2} \\ d^{(\mathrm{e})}_{3(i-1)+3} \end{Bmatrix} \tag{60}$$

and for $i=\{4,5,6\}$

$$d_{(i)} = w^{(i)}_{,n} = d^{(\mathrm{e})}_{i+6} \tag{61}$$

The three extra degrees of freedom at C are

$$\begin{Bmatrix} d^{(\mathrm{e})}_{13} \\ d^{(\mathrm{e})}_{14} \\ d^{(\mathrm{e})}_{15} \end{Bmatrix} = \begin{Bmatrix} w \\ -w_{,1} \\ -w_{,2} \end{Bmatrix}_{C} \tag{62}$$

[1]The conditions $w^{[3]}=w^{[1]}$, $-w^{[3]}_{,1}=-w^{[1]}_{,1}$ and $-w^{[3]}_{,2}=-w^{[1]}_{,2}$ are redundant and dependent from those indicated, hence they shall not be used.

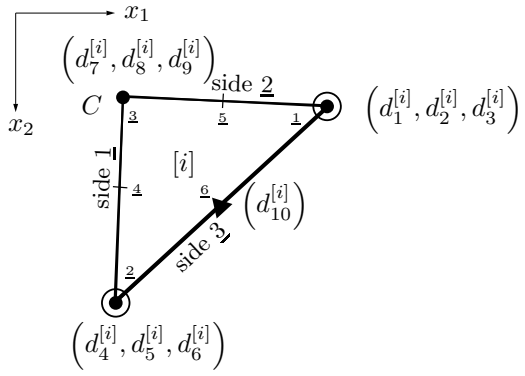

Figure 6: $[i]$ subelement's degrees of freedom of the HCT12 element.

Once again, area coordinates will be used to form the approximation in the subelements. A complete cubic base might be chose as

$$\mathbf{P} = \begin{bmatrix} L_1^3 & L_2^3 & L_3^3 & L_1^2 L_2 & L_1^2 L_3 & L_2^2 L_3 \\ & & & L_1 L_2^2 & L_1 L_3^2 & L_2 L_3^2 & L_1 L_2 L_3 \end{bmatrix} \tag{63}$$

In figure 6 the degrees of freedom associated to each local node of the $[i]$ subelement are depicted.

Each subelement will have an approximation for the displacement's field, in area coordinates, given by

$$w^{[i]}(L_1, L_2, L_3) = \mathbf{P}(L_1, L_2, L_3)\, \boldsymbol{\alpha}^{[i]} \tag{64}$$

with the vector that groups the approximation weights in each subelement, $\boldsymbol{\alpha}^{[i]}$, given by

$$\boldsymbol{\alpha}^{[i]T} = \begin{Bmatrix} \alpha_1 & \alpha_2 & \alpha_3 & \dots & \alpha_{10} \end{Bmatrix} \tag{65}$$

Therefore, the relation between $\boldsymbol{\alpha}^{[i]}$ and the vector that groups the degrees of freedom, $\mathbf{d}^{[i]}$, can be grouped in matrix form. For each subelement we have

$$\mathbf{d}^{[i]} = \mathbf{A}^{[i]}\, \boldsymbol{\alpha}^{[i]} \Leftrightarrow \boldsymbol{\alpha}^{[i]} = \mathbf{A}^{[i]-1} \mathbf{d}^{[i]} \tag{66}$$

where the displacement field is

$$w^{[i]} = \mathbf{P}\mathbf{A}^{[i]-1}\mathbf{d}^{[i]} \Leftrightarrow w^{[i]} = \boldsymbol{\Psi}^{[i]}\mathbf{d}^{[i]} \tag{67}$$

The $\boldsymbol{\Psi}^{[i]}$ matrix was explicitly evaluated as a function of the b_i, c_i and $A^{[i]}$ parameters and the area coordinates L_1, L_2 and L_3.

In order to impose the continuity of the normal derivative, the evaluation of the normal derivative in the $\underline{4}$ and $\underline{5}$ nodes is also needed:

$$w^{[i]}_{,\underline{n}^{\alpha+3}} = -\frac{l_{\underline{\alpha}}}{2A^{[i]}} \left(\frac{\partial w}{\partial L_1} + p_{\underline{\alpha}} \frac{\partial w}{\partial L_2} + q_{\underline{\alpha}} \frac{\partial w}{\partial L_3} \right) \Bigg|_{\left(L_1^{\underline{\alpha}}, L_2^{\underline{\alpha}}, L_3^{\underline{\alpha}}\right)} \tag{68}$$

This derivatives are explicitly evaluated as a function of b_i, c_i and $A^{[i]}$. Constants $p_{\underline{\alpha}}$ and $q_{\underline{\alpha}}$ are given in Sanches (2011, page 33).

The expressions given by (58) can be written in matrix form considering the degrees of freedom that are free, $\mathbf{d}_f^{(\mathrm{e})}$, and restrained, $\mathbf{d}_c^{(\mathrm{e})}$,

$$\begin{aligned}\mathbf{G}^{(\mathrm{e})}\mathbf{d}_c^{(\mathrm{e})} + \mathbf{H}^{(\mathrm{e})}\mathbf{d}_f^{(\mathrm{e})} = 0 \Leftrightarrow \\ \Leftrightarrow \mathbf{d}_c^{(\mathrm{e})} = -\mathbf{G}^{(\mathrm{e})-1}\mathbf{H}^{(\mathrm{e})}\mathbf{d}_f^{(\mathrm{e})} \Leftrightarrow \\ \Leftrightarrow \mathbf{d}_c^{(\mathrm{e})} = \mathbf{U}^{(\mathrm{e})}\mathbf{d}_f^{(\mathrm{e})}\end{aligned} \tag{69}$$

where

$$\mathbf{d}_f^{(\mathrm{e})T} = \begin{Bmatrix} d_1^{(\mathrm{e})} & d_2^{(\mathrm{e})} & d_3^{(\mathrm{e})} & \dots & d_{12}^{(\mathrm{e})} \end{Bmatrix} \tag{70a}$$

$$\mathbf{d}_c^{(\mathrm{e})T} = \begin{Bmatrix} d_{13}^{(\mathrm{e})} & d_{14}^{(\mathrm{e})} & d_{15}^{(\mathrm{e})} \end{Bmatrix} \tag{70b}$$

$\mathbf{U}^{(\mathrm{e})}$ is the restriction's matrix given by

$$\mathbf{U}^{(\mathrm{e})} = -\mathbf{G}^{(\mathrm{e})-1}\mathbf{H}^{(\mathrm{e})} \tag{71}$$

The evaluation of the displacements field inside each subelement is possible after the evaluation of the center displacements, $\mathbf{d}_c^{(\mathrm{e})}$, using equation (69).

5.2 Element Stiffness Matrix

As seen for this element, the approximation functions are cubic, hence the curvatures are linear and a complete base in area coordinates is

$$\mathbf{L} = \begin{bmatrix} L_1 & L_2 & L_3 \end{bmatrix} \tag{72}$$

The procedure to obtain the stiffness matrix is very similar to that shown for the T21 element. In this case, however, the matricial entities have different dimensions – we have less degrees of freedom – and the procedure is made for each subelement in particular. The three elemental matrices obtained for each subelement are then assembled in the element stiffness matrix, $\mathbf{K}^{(\mathrm{e})}$, as usual. This matrix, however, will have a (15×15) dimension since it includes the free degrees of freedom at the center. The consequence is an non-compatible element since the normal derivative of an internal subelement side is quadratic and only the normal derivatives of that side vertexes were imposed. To generate a compatible element, the restriction given by (69) has to be enforced.

The FEM equations system can be written as

$$\mathbf{K}^{(\mathrm{e})}\mathbf{d}^{(\mathrm{e})} = \mathbf{f}^{(\mathrm{e})} + \mathbf{r}^{(\mathrm{e})} \tag{73}$$

where $\mathbf{r}^{(\mathrm{e})}$ is a vector that groups two force vectors, $\mathbf{r}_c^{(\mathrm{e})}$ and $\mathbf{r}_f^{(\mathrm{e})}$, corresponding to the restrained and free degrees of freedom, respectively. The resultant of this vectors has to be null, and it can be show that

$$\mathbf{r}_f^{(\mathrm{e})} = -\mathbf{U}^{(\mathrm{e})T}\mathbf{r}_c^{(\mathrm{e})} \tag{74}$$

resulting the final element stiffness matrix, with (12×12) dimension and the element equivalent nodal force vector for the HCT12 element

$$\begin{aligned}\mathbf{K}^{(\mathrm{e})} = \mathbf{K}_{ff}^{(\mathrm{e})} + \mathbf{K}_{fc}^{(\mathrm{e})}\mathbf{U}^{(\mathrm{e})} + \mathbf{U}^{(\mathrm{e})T}\mathbf{K}_{cf}^{(\mathrm{e})} + \\ + \mathbf{U}^{(\mathrm{e})T}\mathbf{K}_{cc}^{(\mathrm{e})}\mathbf{U}^{(\mathrm{e})}\end{aligned} \tag{75a}$$

$$\mathbf{f}^{(\mathrm{e})} = \mathbf{f}_f^{(\mathrm{e})} + \mathbf{U}^{(\mathrm{e})T}\mathbf{f}_c^{(\mathrm{e})} \tag{75b}$$

5.3 Element Force Vector

The evaluation of the element force vector follows the same procedures of those used previously. Once again, like it was done with the stiffness matrix, the vectors' construction is made at the subelement level and then assembled to the element.

Like the T21 element, the HCT12 has six nodes which allows the definition of quadratic loads in the two-dimensional space. Therefore, the quadratic polynomial base $\mathbf{P}^Q$ defined in (33) and the $\mathbf{Y}^Q$ matrix are the same. The approximation's base is that defined in (63) and the $\mathbf{A}^{[i]}$ matrix that relates the degrees of freedom and the approximation's weights is that used in (66).

In each subelement, the force vector that groups the quadratic effective load, $\mathbf{f}_{\overline{p}_{ef}}^{[i]}$, is similar to that shown in (36), namely

$$\mathbf{f}_{\overline{p}_{ef}}^{[i]} = A^{[i]}\mathbf{A}^{[i]-T}\mathbf{Z}\,\mathbf{Y}^Q\overline{\mathbf{p}}_{ef}^{[i]} \tag{76}$$

Likewise, the subelement force vector due to a quadratic temperature variation, $\mathbf{f}_{\Delta T}^{[i]}$, can be obtained similarly to (42)

$$\begin{aligned}\mathbf{f}_{\Delta T}^{[i]} = \frac{1}{4A^{[i]}}\frac{\alpha}{h}\Big(\mathbf{Q}_{11}^{[i]T}\mathbf{M}\left(D_{11}^{[i]} + D_{12}^{[i]}\right) + \\ + \mathbf{Q}_{22}^{[i]T}\mathbf{M}\left(D_{21}^{[i]} + D_{22}^{[i]}\right)\Big)\mathbf{Y}^Q\Delta\mathbf{T}^{[i]}\end{aligned} \tag{77}$$

5.4 Element Compatibility

In the subdomain, the displacement's field approximation is generated by a polynomial, therefore the displacement itself and all its derivatives are continuous. This implies the compatibility since, in the subdomain, the element is C^∞.

Since the approximation for the displacement's field is cubic, four parameters are needed to ensure compatibility along all sides. These are the displacement and tangential derivative on the two vertexes of each side. The normal derivative on the subelements' sides is quadratic, so three parameters are needed to define it along the three interior element sides. In the central, C, and vertex, (i), nodes the normal derivative is imposed. The third condition is also the normal derivative in the middle of the respective side, as it shown in figure 7. Since the degrees of freedom associated with the interior sides are the same as those involved in the sides between elements, this demonstration proves not only

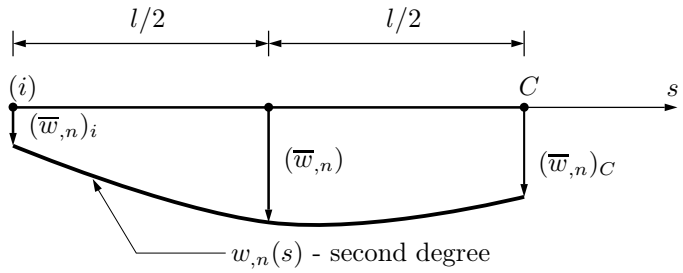

Figure 7: Quadratic variation of the normal derivative, $w_{,n}$, on the interior side of the HCT12 element.

the compatibility on the the boundary between subelements but also on the boundary between elements.

In order to satisfy the compatibility conditions on the kinematic boundary, there are some differences that need to be accounted for. It is important to remaind that the degrees of freedom of this element do not include curvatures – only displacements and first order partial derivatives. Therefore, in general, in a simply supported edge we have $w = 0$ and $(-w_{,t}) = 0$. In a sliding clamped edge we shall only impose $(-w_{,n} = 0)$, while in a clamped edge we have $w = 0$ e $(-w_{,n}) = 0$.

6 HCT9 Element Formulation

6.1 Approximation Functions

As seen before for the T18 element, the HCT9 element also derives from a more elaborated element, in this case, the HCT12, by eliminating some nodes, which are, once again, the mid-side nodes. Therefore, we have a three node element with three degrees of freedom by node, namely, w, $(-w_{,1})$ and $(-w_{,2})$, in a total of nine. In this case we also use the division of the element in three subelements. This element was first proposed in Clough and Tocher (1966).

The approximation inside of the element is formed by the same ten parameters as in the case of the HCT12. This will also be cubic and a complete base in area coordinates is show in (63). In each $[i]$ subelement we'll have the approximation defined by (64).

Therefore, the degrees of freedom in each subelement are the same ten presented in figure 6. However, in this case it is imposed that the normal derivative along the sides of the element has a linear variation – see figure 8 – and not quadratic as previously, *i.e.*

$$w_{,n}^{[i]}(s) = a_0 + a_1 s = \mathbf{S}\,\mathbf{a}^{[i]} \tag{78}$$

with

$$\mathbf{S} = \begin{bmatrix} 1 & s \end{bmatrix} \tag{79}$$

and

$$\mathbf{a}^{(\mathrm{e})T} = \begin{bmatrix} a_0 & a_1 \end{bmatrix} \tag{80}$$

The evaluation of $(\overline{w}_{,n})_{\underline{6}}$ is now obvious

$$(\overline{w}_{,n})_{\underline{6}} = \frac{1}{2}\left((\overline{w}_{,n})_{\underline{1}} + (\overline{w}_{,n})_{\underline{2}}\right) \tag{81}$$

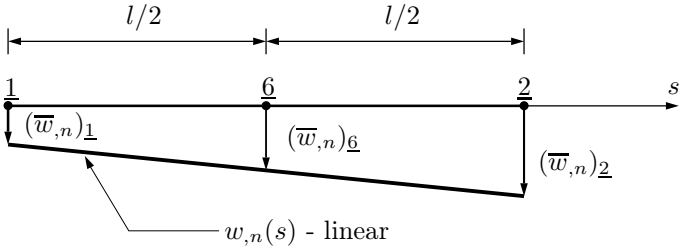

Figure 8: Linear variation of the normal derivative, $w_{,n}$, in the HCT9 element side.

The excessive degree of freedom, $d_{10}^{[i]} = (\overline{w}_{,n})_{\underline{6}}$, can be written as a function of the free degrees of freedom, $\mathbf{d}_f^{[i]}$, by

$$d_{10}^{[i]} = \mathbf{G}\,\mathbf{d}_f^{[i]} \tag{82}$$

where $\mathbf{G}$ is a restriction matrix.

In the $\underline{\alpha} = \{1, 2\}$ nodes that form the sides $\underline{3}$ of each subelement we have

$$\begin{aligned}(w_{,n})_{\underline{3}} &= -\left((n_1)_{\underline{3}}\,(-w_{,1})_{\underline{3}} + (n_2)_{\underline{3}}\,(-w_{,2})_{\underline{3}}\right) = \\ &= -\left((n_1)_{\underline{3}}\,d^{[i]}_{3(\underline{\alpha}-1)+2} + (n_2)_{\underline{3}}\,d^{[i]}_{3(\underline{\alpha}-1)+3}\right)\end{aligned} \tag{83}$$

Therefore, the relation (81) can be rewritten and the $\mathbf{G}$ matrix assumes the form

$$\mathbf{G} = -\frac{1}{2}\begin{bmatrix} 0 & (n_1)_{\underline{3}} & (n_2)_{\underline{3}} & 0 & (n_1)_{\underline{3}} & (n_2)_{\underline{3}} & 0 & 0 & 0 \end{bmatrix} \tag{84}$$

The approximation functions can now be determined

$$\begin{aligned} w^{[i]} = \mathbf{\Psi}^{[i]}\mathbf{d}^{[i]} &= \begin{bmatrix} \mathbf{\Psi}_f^{[i]} & \psi_{10}^{[i]} \end{bmatrix} \begin{Bmatrix} \mathbf{d}_f^{[i]} \\ d_{10}^{[i]} \end{Bmatrix} = \\ &= \mathbf{\Psi}_f^{[i]}\mathbf{d}_f^{[i]} + \psi_{10}^{[i]} d_{10}^{[i]} = \mathbf{\Psi}_f^{[i]}\mathbf{d}_f^{[i]} + \psi_{10}^{[i]}\mathbf{G}\,\mathbf{d}_f^{[i]} = \\ &= \left[\mathbf{\Psi}_f^{[i]} + \psi_{10}^{[i]}\mathbf{G}\right]\mathbf{d}_f^{[i]} = \mathbf{\Psi}_{\mathrm{HCT9}}^{[i]}\mathbf{d}_f^{[i]} \end{aligned} \tag{85}$$

where

$$\mathbf{\Psi}_{\mathrm{HCT9}}^{[i]} = \mathbf{\Psi}_f^{[i]} + \psi_{10}^{[i]}\mathbf{G} \tag{86}$$

and the relation between the vector that groups the nodal displacements and its derivatives in the HCT12 subelements, $\mathbf{d}^{[i]}$, with the homonymous of the HCT9 element, $\mathbf{d}_{\mathrm{HCT9}}^{[i]}$, is given by

$$\mathbf{d}^{[i]} = \begin{Bmatrix} \mathbf{d}_f^{[i]} \\ d_{10}^{[i]} \end{Bmatrix} = \begin{bmatrix} \mathbf{I}_9 \\ \mathbf{G} \end{bmatrix}\mathbf{d}_f^{[i]} = \mathbf{G_I}\,\mathbf{d}_{\mathrm{HCT9}}^{[i]} \tag{87}$$

where $\mathbf{I}_9$ is the identity matrix with (9×9) dimension.

6.2 Element Stiffness Matrix

The expression to evaluate the element stiffness matrix is the same given in (75a) where the matrices involved have different dimensions. The stiffness submatrix of the free degrees of freedom now has (9×9) dimension and the submatrix of the restrained degrees of freedom has (3×3). The relation given by (71) is still applied to impose the continuity of the normal derivatives in the interior sides of the element.

6.3 Element Force Vector

Like already seen for the T18 element, the HCT9 only allows defining linear loads in the two-dimensional space since it only has three nodes. Once again, there's nothing new worth to be shown besides mentioning the changes in the matrices dimensions. As an example we show here the **M** matrix symbolically evaluated

$$\mathbf{M} = \frac{1}{12}\begin{bmatrix} 2 & 1 & 1 \\ 1 & 2 & 1 \\ 1 & 1 & 2 \end{bmatrix} \tag{88}$$

6.4 Element Compatibility

The compatibility analysis for this element is very similar to that made for the HCT12. The difference is in the linear normal derivative along the sides that, along with the imposition of the normal derivatives in the vertexes, allows the obtention of all the parameters that define the cubic approximation for the displacement's field.

7 Numerical example

7.1 Distortion Test

This test is referenced in, *e.g.*, Batoz and Tahar (1982, page 1665) and its objective is the assessment of the elements' quality when subjected to distortion. A rectangular plate with dimensions $(L \times 1)$, with $L = \{1, 2, 3 \ldots 12\}$ is clamped in one of the smaller edges and loaded with unitary opposite loads on the opposite vertexes. The structure is evaluated resorting only to two elements and the displacements are then measured on the vertexes where the loads are applied. To have some conclusions, a reference solution has to be generated. In this case we used a T21 element mesh where the elements had a characteristic dimension, $h = 0.25$, regardless of the value of L. Also, this mesh was symmetrical relatively to $x_2 = 0.5$.

The results for this test are shown for all four elements in figure 9. There it is possible to see that the T21 and T18 show very good results, very near to the reference solution. In the HCT12 we notice some loss of quality but still the results are very acceptable. On the other hand, the HCT9 element presented inferior results showing a poorer quality.

7.2 Simply Supported Plate

In order to verify the formulation and implementation of the elements, a rectangular simply supported plate with a unit uniform effective load is tested. The exact solution for this problem is given in Timoshenko and Woinowsky-Krieger (1959, chapter 5, page 105). To reduce the computational process two symmetry simplification are made. The result is a rectangular plate with two supported and two sliding clamped edges.

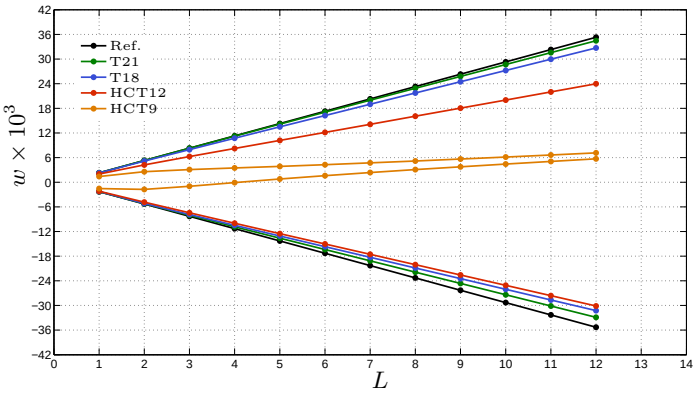

Figure 9: Performance of the elements on the distortion's test.

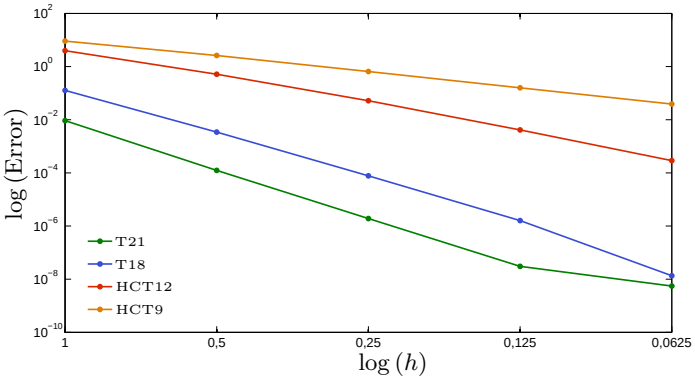

Figure 10: Deformation's energy error as a function of the characteristic dimension of the elements.

The deformation's energy is evaluated through

$$U = \frac{1}{2}\sum_{(\mathrm{e})} \mathbf{d}^{(\mathrm{e})T}\mathbf{K}^{(\mathrm{e})}\mathbf{d}^{(\mathrm{e})} \tag{89}$$

Representing its value for each mesh of each element as a function of the elements' characteristic dimension, h, in a double logarithmic scale, we'll obtain, approximately, straight lines whose slopes are the convergence ratio of the elements. This graphical representations and the numerical values of the ratios are presented in figure 10 and table 1, respectively.

From this results we can take similar conclusion to those obtained with distortion's test: the T21 and the T18 elements present better results. In fact, the T21 element has a convergence ratio three times higher than the one registered for the HCT9, clearly, the element with the lowest quality.

As an example, are also shown in figure 11 the diagrams

T21	T18	HCT12	HCT9
6.1	5.4	3.4	2.0

Table 1: Convergence ratios for the four elements.

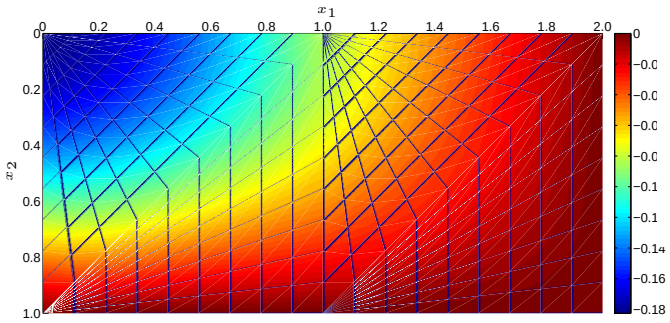

(a) T21 element.

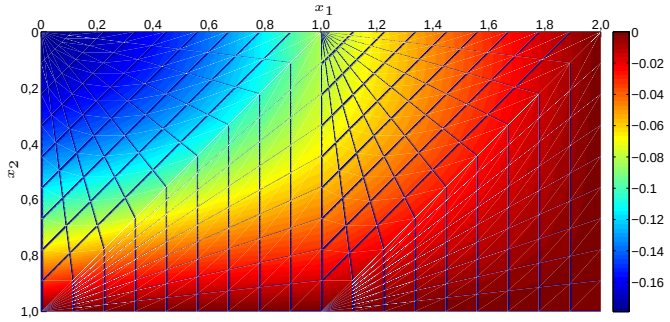

(b) T18 element.

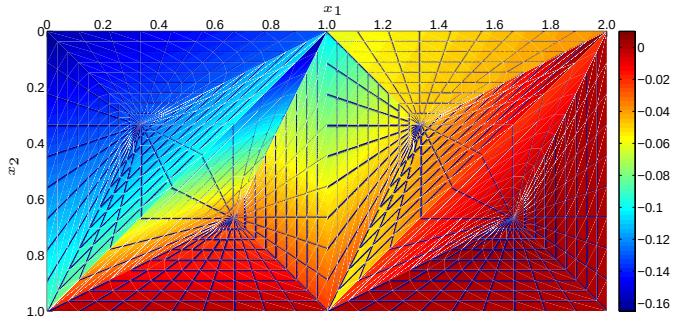

(c) HCT12 element.

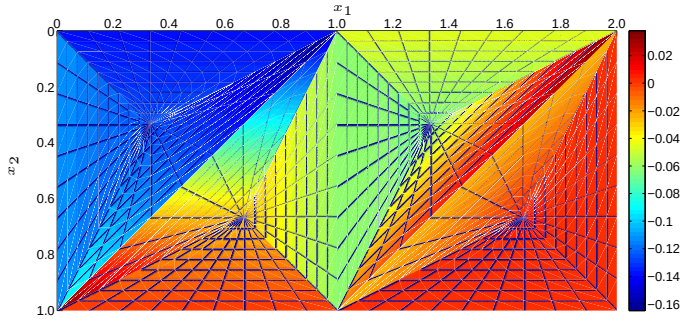

(d) HCT9 element.

Figure 11: Torsional moment m_{12} obtained for the four elements with the less refined mesh.

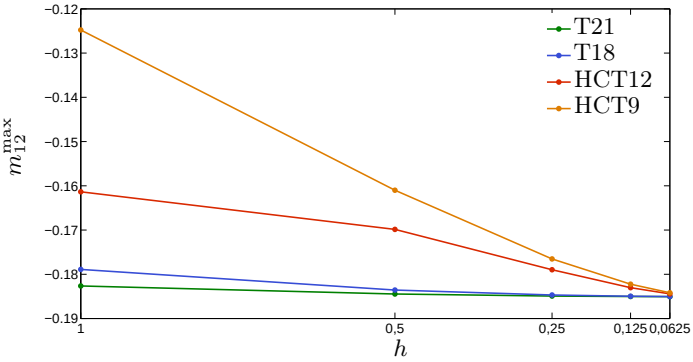

Figure 12: Maximum torsional moment's, m_{12}^{max}, convergence in the center of the rectangular plate, for the four elements.

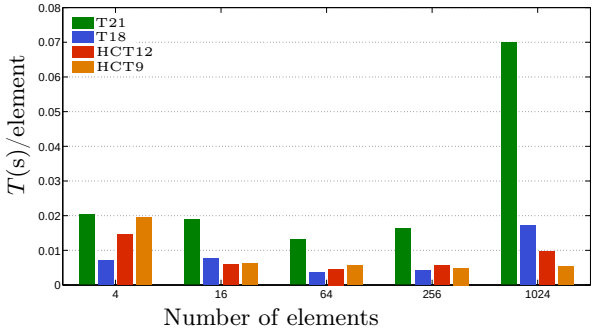

Figure 13: Computational times taken by the elements.

for the torsional moment, m_{12}, in the case of the less refined mesh (only four elements). Also its convergence is shown in figure 12. Once again, the T21 and T18 elements have smoother diagrams and their torsional moment values converge more rapidly to the exact solution.

An assessment on computational times was also performed. In figure 13 the times taken by the program for each element to perform all the elementary calculations, for all the meshes analyzed, are shown.

8 Conclusions

All four elements showed satisfactory results, always converging to the exact solutions. In the majority of the examples tested, the T21 and T18 elements were the ones delivering the better solutions. Even with lower refinement levels, this two elements presented high quality results.

Higher quality solutions are also achievable with the HCT elements. However, the refinement has to increase substantially, with consequences on times taken by the program to perform all the calculations.

From the engineer point of view, the HCT9 element might be the easiest one to work with, as its degrees of freedom are the standard ones in plate analysis. Also the connection with other structural elements is, in this case, simpler.

The downside of the T21 element is the high number of

nodes, mainly because of the mid-side ones. Removing this nodes proved to be a more efficient way to obtain solutions with high quality, as assessed with the T18 element.

Therefore, considering the computacional costs and the quality of the obtained solutions we are led to conclude that the T18 element is the one that presents better results. Its solutions are slightly inferior to those presented by the T21 element, however it takes less time to generate those solutions, specially in highly refined meshes.

References

Argyris, J. H., I. Fried and D. W. Scharpf (1968). The TUBA family of plate elements for the matrix displacement method. *The Aeronautical Journal of the Royal Aeronautical Society*, *72*(692), 701–709.

Batoz, J.-L. and M. B. Tahar (1982). Evaluation of a new quadrilateral thin plate bending element. *International Journal for Numerical Methods in Engineering*, *18*(11), 1655–1677.

Bell, K. (1969). A refined triangular plate bending finite element. *International Journal for Numerical Methods in Engineering*, *1*(1), 101–122.

Clough, R. W. and C. A. Felippa (1969). A refined quadrilateral element for analysis of plate bending. In L. Berke, R. M. Bader, W. J. Mykytow, J. S. Przemieniecki and M. H. Shirk (Editors) *Proceedings of the Second Conference on Matrix Methods in Structural Mechanics held at Wright-Patterson Air Force Base, Ohio, 15-17 October, 1968*, pages 399–440. Air Force Dynamics Laboratory. AFFDL-TR-68-150.

Clough, R. W. and J. L. Tocher (1966). Finite element stiffness matrices for analysis of plate bending. In J. S. Przemieniecki, R. M. Bader, W. F. Bozich, J. R. Johnson and W. J. Mykytow (Editors) *Matrix Methods in Structural Mechanics, Proceedings of the Conference held at Wright Patterson Air Force Base, Ohio, on 26-28 October, 1965*, pages 515–545. Air Force Flight Dynamics Laboratory. AFFDL-TR-66-80.

MATLAB (2010). *MATLAB, The Language of Technical Computing*. The MathWorks Inc. Version 7.11.

Sanches, Pedro (2011). *Elementos finitos triangulares compatíveis na análise estrutural de lajes finas*. Master's thesis, Instituto Superior Técnico, Universidade Técnica de Lisboa.

Timoshenko, S. P. and S. Woinowsky-Krieger (1959). *Theory of Plates and Shells*. McGraw–Hill, second edition.

Wolfram Research, Inc. (2010). *Mathematica Edition: Version 8.0*. Wolfram Research, Inc., Champaign, Illinois.

Zienkiewicz, O. C., R. L. Taylor and J. Z. Zhu (2005). *Finite Element Method: Its Basis and Fundamentals*, volume 1. Elsevier Butterworth–Heinemann, sixth edition.